JBIC Journal of Biological Inorganic Chemistry (2020) 25:509–519
https://doi.org/10.1007/s00775-020-01779-y

ORIGINAL PAPER

Multi-target heteroleptic palladium bisphosphonate complexes

Micaella Cipriani[1] · Santiago Rostán[1] · Ignacio León[2] · Zhu-Hong Li[3] · Jorge S. Gancheff[1] · Ulrike Kemmerling[4] · Claudio Olea Azar[5] · Susana Etcheverry[2] · Roberto Docampo[3] · Dinorah Gambino[1] · Lucía Otero[1]

Received: 20 December 2019 / Accepted: 16 March 2020 / Published online: 30 March 2020

Abstract

Bisphosphonates are the most commonly prescribed drugs for the treatment of osteoporosis and other bone illnesses. Some of them have also shown antiparasitic activity. In search of improving the pharmacological profile of commercial bisphosphonates, our group had previously developed first row transition metal complexes with *N*-containing bisphosphonates (NBPs). In this work, we extended our studies to heteroleptic palladium–NBP complexes including DNA intercalating polypyridyl co-ligands (NN) with the aim of obtaining potential multi-target species. Complexes of the formula $[Pd(NBP)_2(NN)]\cdot 2NaCl\cdot xH_2O$ with NBP = alendronate (ale) or pamidronate (pam) and NN = 1,10 phenanthroline (phen) or 2,2′-bipyridine (bpy) were synthesized and fully characterized. All the obtained compounds were much more active in vitro against *T. cruzi* (amastigote form) than the corresponding NBP ligands. In addition, complexes were nontoxic to mammalian cells up to 50–100 µM. Compounds with phen as ligand were 15 times more active than their bpy analogous. Related to the potential mechanism of action, all complexes were potent inhibitors of two parasitic enzymes of the isoprenoid biosynthetic pathway. No correlation between the anti-*T. cruzi* activity and the enzymatic inhibition results was observed. On the contrary, the high antiparasitic activity of phen-containing complexes could be related to their ability to interact with DNA in an intercalative-like mode. These rationally designed compounds are good candidates for further studies and good leaders for future drug developments.

Graphic abstract

Four new palladium heteroleptic complexes with *N*-containing commercial bisphosphonates and DNA intercalating polypyridyl co-ligands were synthesized and fully characterized. All complexes displayed high anti-*T. cruzi* activity which could be related to the inhibition of the parasitic farnesyl diphosphate synthase enzyme but mainly to their ability to interact DNA.

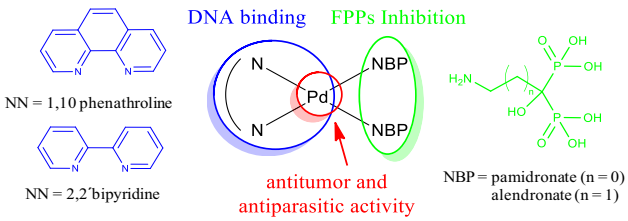

Keywords Bisphosphonate · Palladium · DNA · Chagas · Toxoplasmosis

Introduction

Bisphosphonates are structural analogs of inorganic pyrophosphate that are resistant to enzymatic and chemical breakdown. These compounds are well-established drugs for the prevention and treatment of diseases associated with excessive bone resorption, including Paget's disease of bone,

Electronic supplementary material The online version of this article (https://doi.org/10.1007/s00775-020-01779-y) contains supplementary material, which is available to authorized users.

✉ Lucía Otero
luotero@fq.edu.uy

Extended author information available on the last page of the article

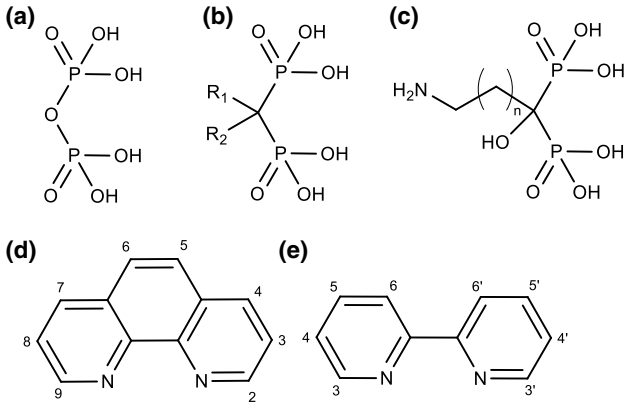

Fig. 1 Top: **a** pyrophosphate; **b** general structure of bisphosphonates; **c** pamidronate (pam, $n=1$, acid form), alendronate (ale, $n=2$, acid form); Bottom: polypyridyl compounds (NN = 1,10-phenanthroline (phen, (**d**)), 2,2-bipyridine (bpy, (**e**))

myeloma, bone metastases, and osteoporosis [1]. The chemical structure of bisphosphonates (Fig. 1) allows changes in the two lateral chains (R_1 and R_2) leading to variations in physicochemical and biological properties as well as to different mechanisms of action. The simplest, non-nitrogen-containing bisphosphonates can be metabolically incorporated as non-hydrolysable analogs of adenosine triphosphate (ATP). In contrast, the more potent nitrogen-containing bisphosphonates (NBPs) inhibit a key enzyme in the mevalonate pathway, farnesyl pyrophosphate synthase (FPPS), leading to osteoclast apoptosis [2–4].

NBPs are also potent inhibitors of the proliferation of trypanosomatid (*Trypanosoma cruzi*, *Trypanosoma brucei rhodesiense and Leishmania donovani*) and Apicomplexan (*Toxoplasma gondii and Plasmodium falciparum*) parasites [5–7]. These parasites have some organelles called acidocalcisomes that are equal in composition to bone mineral and that could accumulate bisphosphonates aiding to their antiparasitic activity [8]. In addition, the isoprenoid biosynthesis is also the antiparasitic target of NBPs through the inhibition of the enzymatic activity of FPPS [9–11].

Our group had previously developed first row transition metal complexes with some commercial NBPs, i.e., risedronate, alendronate, pamidronate and ibandronate in the search of more effective anti-*Trypanosoma cruzi* (*T. cruzi*) agents. Obtained compounds showed IC_{50} values in vitro against the amastigote form of the parasite in the low micro molar levels with low toxicity on mammalian *Vero* cells. As a consequence of metal complexation, the activity of the free NBPs increased and the obtained complexes were able to selectively inhibit *T. cruzi* FPPS [12–14].

Based on these results, we have decided to rationally design multi-target metal complexes including NBPs as ligands with the purpose of developing new potential anti-*T. cruzi* agents. Metal complexes are ideal candidates for a multi-target therapy by designing a single chemical entity that acts simultaneously on multiple targets through, not only the metal, but the different coordinated ligands [15, 16] (Fig. 2). Palladium was selected as metal center and, besides NBPs, polypyridyl compounds (NN, Fig. 1) were chosen as ligands. On the one hand, as stated, parasitic FPPS enzyme could be a potential target for the proposed complexes as it is for the free NBPs and these ligands would contribute to the selectivity of the compounds through accumulation in acidocalcisomes [8]. On the other hand, the selection of both the metal ion and the NN co-ligands is intended for pointing out DNA as target. The reason why this biomolecule could be a potential parasitic target is based on that DNA has classically been involved in the mode of action of metal-based anticancer compounds [17]. Due to the observed metabolic similarities between tumor cells and parasites, a parallelism between the antitumor and antiparasitic effects has been proposed [18–21]. In particular, as an alternative to the classic covalent DNA interaction, metal complexes with extended planar aromatic ligands can also bind reversibly to DNA through intercalation of the planar aromatic moiety between nucleobases [22, 23]. The most widely investigated intercalating ligands are derivatives of 2,2′-bipyridine (bpy) or 1,10-phenanthroline (phen). In addition, some of us had demonstrated that metal complexes with this kind of ligands also showed antiparasitic activity [24–26].

The selection of palladium as the metal center for the proposed complexes is based on that Pd(II) complexes have been widely studied as an alternative to Pt(II) ones in cancer therapy [27]. In addition, both palladium and platinum complexes have shown activity against trypanosomatid parasites [28–30]. Besides the chemical resemblance between both metal ions, Pd(II) complexes are kinetically less stable than their Pt(II) analogs tending to dissociate readily in solution leading to toxicity. To stabilize Pd(II) complexes, chelating ligands are often envisaged and in particular, NN heterocyclic derivatives [31]. Moreover, as Pd(II) ions usually adopt square planar geometries, planarity of the ligands could be extended to the square planar complex making the complex more susceptible to intercalate in DNA [32].

In this work, four new complexes of the formula [Pd(NN)$(NBP)_2$] with NN = 2,2-bipyridine (bpy) or 1,10-phenanthroline (phen) (Fig. 1) and NBP = alendronate or pamidronate

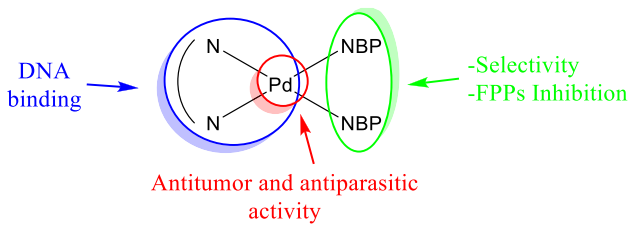

Fig. 2 Rational design of proposed multi-target palladium complexes

(Fig. 1) were synthesized and fully characterized in the solid state and in solution. Computational studies at the density functional level of theory (DFT) were performed to calculate the vibrational spectra of the complexes at the optimized geometries. The in vitro antiproliferative effect of the obtained compounds on *T. cruzi* amastigotes, their ability to inhibit two parasitic enzymes of the mevalonate pathway and to interact with DNA were evaluated. Additionally, activity on *Toxoplasma gondii* (*T. gondii*) parasite and preliminary anticancer activity were also studied.

Materials and methods

Materials

All common laboratory chemicals were purchased from commercial sources and were used without any further purification. $[PdCl_2(dmso)_2]$ was prepared according to a published procedure [33]. Sodium alendronate trihydrate (4-amino-1-hydroxybutane-1,1-diylphosphonic acid sodium salt, Naale) and sodium pamidronate pentahydrate (3-amino-1-hydroxypropane-1,1-diylphosphonic acid disodium salt, Na_2pam), 2,2-bipyridine (bpy) and 1,10-phenanthroline were purchased from commercial sources and were used as received.

Synthesis of the Pd–NBP–NN complexes

All compounds were prepared by dropwise addition of 5 mL of an aqueous solution containing 0.15 mmol of the NN ligand (bpy or phen) over a solution containing 0.15 mmol of $[PdCl_2(dmso)_2]$ or $Na_2[PdCl_4]$ dissolved in 5 ml of H_2O. The mixture containing a white solid was stirred at room temperature for 1 h and then, 10 mL of an aqueous solution containing 0.30 mmol of the corresponding NBP (Naale o Na_2pam) and 0.30 mmol of triethylamine (TEA) was added dropwise. The mixture was stirred at 60 °C until a clear dark-brown solution was observed and then it was concentrated to 10 mL. The compounds were isolated by adding 10 mL of acetone and washed off with ethyl alcohol and diethyl ether. All the obtained products were microcrystalline yellow solids.

$[Pd(ale)_2(bpy)]\cdot 7H_2O\cdot 2NaCl$, Pd–ale–bpy (yield: 77 mg, 51%). Anal. (%) calc. for $C_{18}H_{46}Cl_2N_4Na_2O_{21}P_4Pd$: C, 21.58; H, 4.63; N, 5.59; H_2O 12.6. Found: C, 21.78; H, 4.63; N, 5.54; H_2O 13.0. ^{1}H-NMR: δ (ppm): 8.39 (d, 2H, H-C6, H-C6′, bpy moiety); 8.00 (t, 2H, H-C4, H-C4′, bpy moiety); 7.85 (d, 2H, H-C3, H- C3′, bpy moiety); 7.44 (t, 2H, H-C5, H-C5′, bpy moiety); 3.10 (m, 4H, N-CH2, ale moiety); 2.12 (m, 8H, N–C–CH2 and N–C–C–CH2, ale moiety); ^{31}P-NMR: δ: 34.8 ppm, 18.5 ppm.

$[Pd(pam)_2(bpy)]\cdot 7H_2O\cdot 2NaCl$, Pd–pam–bpy (yield: 92 mg, 63%). Anal. (%) calc. for $C_{16}H_{42}Cl_2N_4Na_2O_{21}P_4Pd$: C, 19.74; H, 4.35; N, 5.75; H_2O 13.4. Found: C, 20.01; H, 4.25; N, 5.69; H_2O 12.9; ^{1}H-NMR: δ (ppm): 8.56 (d, 1H, H-C6, bpy moiety), 8.34 (t, 1H, H-C5, bpy moiety); 8.23(d, 1H, H-C6′, bpy moiety); 8.23 (d, 1H, H-C3, bpy moiety); 8.00 (t, 1H, H-C5′, bpy moiety); 7.82 (d, 1H, H-C3′, bpy moiety); 7.69 (t, 1H, H-C4, bpy moiety); 7.43 (t, 1H, H-C4′, bpy moiety); 3.38 (m, 4H, N-CH2, pam moiety); 2.31 (m, 4H, N-C-CH2-C, pam moiety); ^{31}P-NMR: δ: 34.8 ppm, 18.6 ppm.

$[Pd(ale)_2(phen)]\cdot 9H_2O\cdot 2NaCl$, Pd–ale–phen (yield: 65 mg, 42%). Anal. (%) calc. for $C_{20}H_{50}Cl_2N_4Na_2O_{23}P_4Pd$: C, 22.62; H, 4.75; N, 5.28; 15.2 H_2O. Found: C, 22.94; H, 4.65; N, 5.38; 15.4 H_2O. ^{1}H-NMR: δ (ppm): 8.42 (d, 2H, H-C2,H-C9, phen mioety); 8.19 (d, 2H, H-C4, H-C7, phen moiety); 7.51 (s, 2H, H-C5, H-C6, phen moiety); 7.35 (dd, 2H, H-C3, H-C8, phen moiety); 3.13 (m, 8H, N-C-CH2-CH2, ale moiety); 2.14 (m, 4H, N-CH2, ale moiety). ^{31}P-NMR: δ: 35.3 ppm, 18.1 ppm.

$[Pd(pam)_2(phen)]\cdot 8H_2O\cdot 2NaCl$, Pd–pam–phen (yield: 67 mg, 44%). Anal. (%) calc. for $C_{18}H_{44}Cl_2N_4Na_2O_{22}P_4Pd$: C, 21.28; H, 4.37; N, 5.52; 14.1 H_2O. Found: C, 21.56; H, 4.25; N, 5.32; 14.1 H_2O. ^{1}H-NMR: δ (ppm): 8.36 (d, 1H, H-C2,phen moiety); 8.17 (t, 2H, H-C3 and H-C8, phen moiety) 8.15 (d, 1H, H-C9, phen moiety) 7.51 (bs, 1H, H-C5, phen moiety); 7.45 (dd, 1H, H-C7, phen moiety); 7.43 (bs, 1H, H-C6, phen moiety); 7.38 (dd, 1H, H-C3, phen moiety); 3.34 (t, 4H, N-CH2, pam moeity); 2.29 (m, 4H, N-C-CH2, pam).^{31}P-NMR: δ: 35.3 ppm, 18.0 ppm.

Physicochemical characterization

C, H and N analyses were carried out with a Thermo Scientific Flash 2000 elemental analyzer. Analytical determination of Na was performed by FAAS on a Perkin Elmer AAnalyst 200 with a 10-cm burner and operated at 589 nm. The hollow cathode lamp (Photron) was operated under the manufacturer's recommendations. The composition of the flame was acetylene (2.5 L/min)–air (10.0 L/min). UV–Vis spectra were recorded in a Shimadzu 1603 spectrophotometer. The FTIR absorption spectra (4000–400 cm^{-1}) of the complexes and free ligands were measured as KBr pellets with a Shimadzu IR Prestige-21 instrument. Thermogravimetric measurements (TGA) were done on a Shimadzu TGA 50 thermobalance, with a platinum cell, working under flowing nitrogen (50 mL min^{-1}) and at a heating rate of 0.5 °C min^{-1} (room temperature to 80 °C range) and 1.0 °C min^{-1} (80–350 °C range). ^{1}H-NMR spectra were recorded with a Bruker Avance 400 MHz spectrometer in D_2O at 27 °C. The peak for residual solvent (H_2O, 4.79 ppm) was used as reference [34]. ^{31}P-NMR spectra were obtained

with the same spectrometer at 161,976 MHz and referred to H_3PO_4 85% (0.00 ppm).

Computational details

All computational studies were performed at the density functional level of theory (DFT). First, pamidronate (as an example) was theoretically studied to shed light on its predominant chemical form in the solid state. The molecular geometry of pam (two isomers) interacting with two sodium atoms and five water molecules (Fig. S1) was optimized employing B3LYP functional [35–37] in combination with 6–31 + G*base [38–41]. Calculations on Pd–pam–phen (taken as example) were conducted aiming at confirming the coordination behavior of pam in these systems. The absence of crystallographic data prompted us to study complexes derived from two different coordination possibilities, i.e., employing *N*-donor atoms (*N*-pam), or *O*-donor atoms (*O*-pam). For the last option, the commonly observed bidentate monoanionic (zwitterionic) form of coordination was supposed [42]. Thus, the geometries of Pd–(*N*-pam)–phen and Pd–(*O*-pam)–phen complexes were optimized in a closed-shell singlet ($S = 1$) employing LANL2DZ base [40, 41, 43–45] on palladium atom, and 6–31 + G*base [38–41] on non-metal atoms. LANL2DZ takes scalar relativistic effects into account, especially important when systems with heavy atoms are studied [46]. Water molecules were included in all cases and for Pd–(*N*-pam)–phen system in particular, two sodium atoms were also added (further details in Fig. 3). The nature of the stationary point was verified through a vibrational analysis (no imaginary frequencies). All theoretical studies reported in this work were conducted by employing the program package Gaussian 09, Rev. A.01 [47].

Biological studies

Drug screening assays in Vero cells and *T. cruzi* intracellular amastigotes

Gamma-irradiated (2000 Rads) Vero cells (3.4×10^4 cells/well) were seeded in 96-well plates (black, clear bottom plates from Greiner Bio-One) in 100 µL RPMI (Roswell Park Memorial Institute from Sigma) with 10% FBS (Fetal Bovine Serum). Gamma irradiation was performed to prevent host cell division and detachment of the culture. Plates were incubated overnight at 35 °C and 7% CO_2. After overnight incubation, Vero cells were challenged with 3.4×10^5 trypomastigotes/well (CL strain overexpressing a tdTomato red fluorescent protein) [48] in 50 µL volume and incubated for 5 h at 35 °C and 7% CO_2. After infection, wells were washed once with Hanks solution (150 µL/well) to eliminate any extracellular parasites and tested compounds were immediately added in serial dilutions in RPMI media in 150 µL volumes and left for the whole period of the experiment. Each dilution was tested in quadruplicate. Each plate also contained controls with host cells and no parasites (for background check), controls with two representative drug dilutions and no parasites (for cytotoxicity assays), and controls with parasites and no drugs (positive control). After drug addition, plates were incubated at 35 °C and 7% CO_2. At day 3 post-infection, plates were assayed for fluorescence. IC_{50} values were determined by non-linear regression analysis using SigmaPlot. Vero cell cytotoxicity was measured by the Alamar blue assay as described previously [49].

Drug screening in *Toxoplasma gondii*

Cell cultures Human foreskin fibroblasts (HFF) (ATCC® SCRC-1041) were grown in Dulbecco's modified Eagle's medium (DMEM) supplemented with 10% fetal bovine serum (FBS) and antibiotics. Cell cultures were maintained at 37 °C in a humidified atmosphere with 5% CO_2 and with replacement of the culture medium every 24–48 h [51].

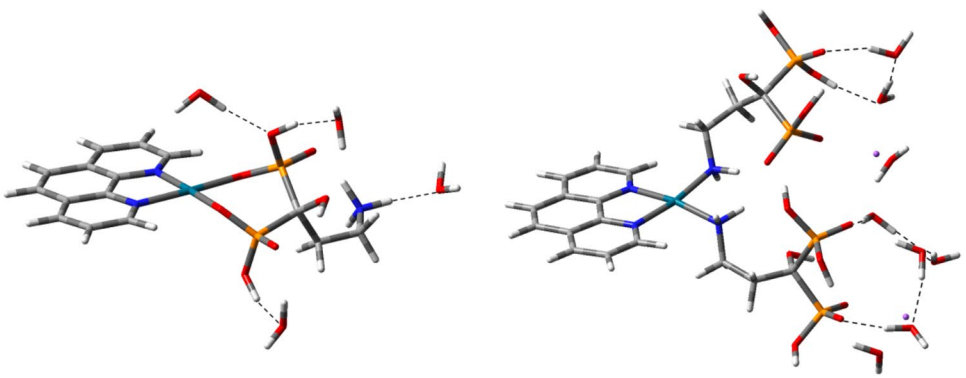

Fig. 3 Model systems $\{[Pd(phen)(O\text{-pam})](H_2O)_4\}^+$ (left), and $\{[Pd(phen)(N\text{-pam})_2](Na)_2(H_2O)_8\}^{2+}$ (right) as calculated at the B3LYP/LANL2DZ/6–31 + G* level ($T = 298$ K)

Parasite culture and harvesting Semi-confluent HFF were infected with *T. gondii* tachyzoites (RH strain) at a multiplicity of infection of 3–5 parasites per cell. After 40 h of infection, infected cells were washed and monolayers were scraped from the flasks and passed through 20-, 23-, and 25-gauge needles. Tachyzoites were purified from host cell debris with a 3.0-µm Isopore filter (Merck Millipore) [51].

Effect of the complexes on tachyzoite viability was evaluated through the tetrazolium salt (MTT) reduction assay (see above). Briefly, 10 mL of 5 mg/mL MTT dye (3[4,5-dimethylthiazol-2-yl]-2,5-diphenyltetrazolium bromide) plus 0.22 mg/mL phenazine methosulfate were added to each well containing 10^6 parasites in 100 mL of RPMI 1640 medium, without phenol red. After incubating the cells for 4 h at 37ºC, the generated formazan crystals were dissolved with 100 mL of 10% (w/v) SDS in 0.01 M HCl. The plates were kept overnight at 37 °C, and the optical density (OD) was determined using a microplate reader (Labsystems Multiskan MS, Finland) at 570 nm. Under these conditions, the OD is directly proportional to the viable cell number in each well. All experiments were performed at least three times.

Preliminary anti-tumor screening

Experimental details on drug screening in MG-63 and A549 tumor cell lines are included in the Supplementary material.

Enzymatic inhibition assays

FPPS assay (both *T. cruzi* and human) Human FPPS (*Hs*FPPS) was expressed and purified as previously described [52, 53]. *T. cruzi* FPPS (*Tc*FPPS) was obtained as described before [9]. The FPPS inhibition radiometric assay was performed essentially as previously reported [53]. Briefly, 100 µL of assay buffer (10 mM Hepes (4-(2-hydroxyethyl)-1-piperazineethanesulfonic acid), pH 7.4, 5 mM $MgCl_2$, 2 mM dithiothreitol, 4.7 µM [4-^{14}C]IPP (isopentenyl diphosphate), 10 µCi/µmol, and 55 µM DMAPP (dimethylallyl pyrophosphate) were prewarmed to 37 °C. The assay was initiated by the addition of recombinant protein (10–20 ng). The assay was allowed to proceed for 30 min at 37 °C and was quenched by the addition of 6 M HCl (10 µL). The reaction media were made alkaline with 6.0 M NaOH (15 µL), diluted in water (0.7 mL), and extracted with hexane (1 mL). The hexane solution was washed with water and transferred to a scintillation vial for counting. One unit of enzyme activity was defined as the activity required to incorporate 1 nmol of [4-^{14}C]IPP into [4-^{14}C]FPP (farnesyl diphosphate) in 1 min. IC_{50} values were determined by non-linear regression analysis using SigmaPlot. 10 µL of several dilutions of the complexes were used for the inhibition assay. Positive (no inhibitor, only enzyme) and negative controls (no inhibitor and no enzyme) for each experiment were performed.

***Tc*SPPS assay** The activity of the enzyme was determined by a radiometric assay. Briefly, 100 µL of assay buffer (100 mM Tris–HCl buffer, pH 7.4, 1 mM $MgCl_2$, 1% (v/v) Triton X-100, 7.07 µM [4-^{14}C]IPP (10 µCi/lmol)) and 50 µM GGPP (geranylgeranyl diphosphate) were prewarmed to 37 °C. The assay was initiated by the addition of 10–20 ng of recombinant protein. The assay was allowed to proceed for 30 min at 37 °C and was quenched by chilling quickly in an ice bath. The reaction products were extracted with 1 mL of 1-butanol saturated with water. The organic layer was washed with water saturated with NaCl, and transferred to a scintillation vial with 4 mL of scintillation solution Ecolume for counting. One unit of enzyme activity was defined as the activity required to incorporate 1 nmol of [4-^{14}C]IPP into [4-^{14}C]FPP in 1 min [54].

DNA interaction studies (fluorescence quenching assay)

Experiments for competitive binding to calf thymus DNA (ctDNA, SIGMA, Type I, No. D-1501) with ethidium bromide (EB, SIGMA) were carried out in 10 mM Tris–HCl buffer at pH 7.4. Millipore® water was used for the preparation of all aqueous solutions. Fluorescence measurements were carried out on individually prepared samples to ensure the same pre-incubation time for all samples in each assay. The complexes' solutions were prepared in purified water followed by appropriate dilution to obtain the targeted concentration. DNA stock solutions were prepared by hydrating ctDNA in Tris–HCl buffer (1 mg/mL, ca. 2 $mMnuc^{-1}$) for 3–4 days at 4 °C, swirling the solution about 4–5 times a day until full dissolution was attained, and a clear solution was obtained. This solution was kept at 4 °C (in the fridge) in-between measurements and discarded after 4 days. The concentration of each stock solution was determined by UV spectrophotometry using the molar extinction coefficient ε (260 nm) = 6600 M^{-1} cm^{-1} nuc^{-1} [55]. An EB 5 mM solution was prepared in Tris–HCl buffer. ctDNA was pre-incubated with EB at 4 °C for 24 h. Samples were prepared with a total concentration of DNA and of EB of 20 µM nuc^{-1} and 10 µM, respectively, by varying the total complex concentration from 2 to 100 µM. They were incubated at 37 °C for 30 min. Samples with complex alone and samples with complex and EB but no DNA were used as blanks. Fluorescence spectra were recorded from 520 to 650 nm at an excitation wavelength of 510 nm with a Shimadzu RF-5301PC spectrofluorometer. Fluorescence emission intensity was corrected for the absorption and emission inner filter effect at the maximum emission wavelength (594 nm) using the

UV–Vis absorption data recorded for each sample according to the following equation [56]:

$$I_{Fcorr} = I_F \times 10^{(Abs(\lambda exc)+Abs(\lambda em)/2}.$$

Results and discussion

Synthesis and solid-state characterization

Four new palladium complexes of the formula $[Pd(NBP)_2(NN)]\cdot 2NaCl\cdot xH_2O$ with NBP = ale or pam and NN = phen or bpy have been synthesized and fully characterized in the solid state and in solution. The new complexes were obtained as yellow microcrystalline solids and all of them were soluble in water. Analytical data, including thermogravimetric analysis results confirmed the proposed formula. The presence of Na^+ in the molecular formula of the compounds neutralizes the charge of some of the non-coordinated phosphonate groups and it was confirmed by atomic absorption measurements (Fig. 4). In fact, the presence of NaCl to stabilize this kind of structure in the solid state had been previously reported for some NBPs [57].

The common synthetic procedure for all the compounds is also shown in Fig. 4. The first step leads to the corresponding $[PdCl_2(NN)_2]$ intermediate insoluble compound. In the second step, a basic medium was used both to dissolve these intermediates by forming μ-hydroxo bridged species [58] and to favor coordination of the bisphosphonate ligands through the terminal ammine nitrogen (see below) [59]. Previously reported palladium–amine–NBP complexes showed dimeric structures with *O*-coordinated bridging NBP ligands [57, 60]. Unlike the compounds included in this work, *O*-coordination of NBP to palladium or other metal centers, leads to water insoluble complexes [12–14, 57, 60]. In addition, *O*-coordination in which the terminal basic amine group is protonated (zwitterion form) was obtained when neutral or acidic synthetic conditions were used. However, *N*-coordination is strongly favored by basic conditions as those used in this work. At high pH values, the amine group deprotonates favoring coordination to the metal center [57, 59].

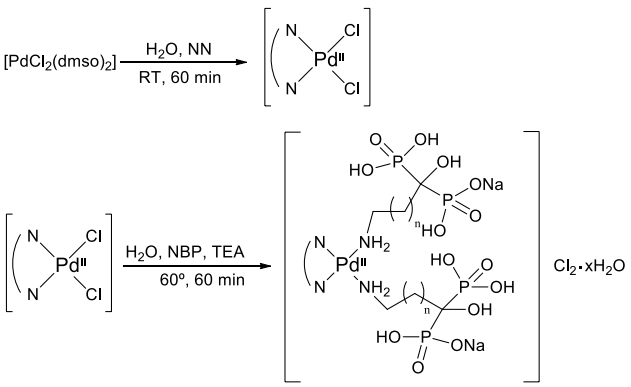

Fig. 4 Synthetic procedure (NN = 2,2-bipyridine (bpy) or 1,10-phenanthroline, NBP = pamidronate ($n = 1$) or alendronate ($n = 2$), *RT* room temperature, *TEA* triethylamine)

FTIR spectra showed characteristic band patterns confirming the presence of the corresponding NN and NBP ligands in the obtained palladium complexes. According to the similarities between the spectra of ale and pam, for each NN ligand, the spectral pattern of Pd–pam–NN and Pd–ale–NN were almost identical (Figure S2). This fact evidences that, in the solid state, the analogous compounds present the same chemical structure. The characteristic bands of the NN ligand corresponding to ν(C = C) and ν(C = N) between 1200 and 1600 cm^{-1} [61] and some of the bisphosphonate ligand bands appear overlapped in the complexes which makes it difficult to do a complete accurate assignment in this spectral region. In fact, DFT calculations (see below) confirmed that most of these bands correspond to coupled vibrational modes. In the region of 900–1300 cm^{-1}, the obtained compounds show the typical band pattern of phosphonates [62]. Modifications in the frequency values of these bands in the complexes could be attributed to sodium and hydrogen bond interactions [12, 13, 63]. The bands near 3350 and 3260 cm^{-1} assigned to $\nu_{as}(NH_2)$ and $\nu_s(NH_2)$, respectively, in the NBP ligands collapse in a broad band as a consequence of coordination through the ammine nitrogen [60]. In addition, the band near 550 cm^{-1} assigned to ν(Pd–O) is not present in the obtained complexes confirming the *N*-coordination of the NBP ligands [60].

The mode of coordination of the NBP ligands in the obtained complexes was also confirmed using a theoretical approach through the analysis of the vibrational spectrum of compounds with *N*- and *O*-coordinated ligands.

Theoretical calculations

As mentioned in 'Computational Details', the absence of crystallographic data for the title complexes motivated theoretical studies on geometry and vibrational IR spectrum. The system involving Pd–pam–phen was selected as an example. Hypothetical compounds with pam coordinated through either nitrogen (Pd–*N*-pam) or oxygen (Pd–*O*-pam) were included in the study.

Vibrational IR spectra of Pd–*O*-pam, and Pd–*N*-pam as calculated at the B3LYP/LANL2DZ/6–31 + G* level in the range 1800–500 cm^{-1} are displayed in Fig. S3, which also exhibits the experimental spectrum. When the theoretical spectra are compared to the experimental evidence, a closer match of the one obtained for Pd–*N*-pam seems to emerge. This observation becomes clearer by inspection of the region

1000–1300 cm^{-1}, in which the absorption-band profile of Pd–*N*-pam system reasonably reproduces the features of the experimental findings. In this region, two main bands with similar intensities were observed both in the calculated Pd–*N*-pam and in the experimental spectra. The origin of these bands can be traced to highly coupled modes involving P–O–H bending, O–P–O stretching and H–N–H wagging modes. In addition, non-negligible contributions from several C=C and C=N stretching bands of the phen ligand were also observed.

The theoretical results already discussed allow us to infer the *N*-coordination mode of pam to Pd^{2+} in the obtained complexes with a 1:2 metal to pam molar ratio. The equilibrium geometry for this system exhibits a slight distorted square planar coordination geometry, being the phen ligand quasi-planar. The interaction of each pam ligand with the metal via *N*-atoms implies that the ligand must change its zwitterionic character to promote coordination leading to a monoanion whose total charge is compensated with a sodium ion (experimentally, this sodium ions are provided by disodium pamidronate). In our model, eight water molecules—that were added to simulate coordination geometry of sodium atoms—were calculated interacting with cations and phosphonate groups through several H-bonds (Fig. 3). It is to be mentioned that no remarkable differences in equilibrium geometry were obtained in going from the gas phase to aqueous solution (taken into account through the C-PCM [64, 65] methodology).

In-solution characterization and stability

^{1}H-NMR spectra in D_2O of all the complexes showed narrow signals typical for diamagnetic square planar palladium(II) complexes (Fig. S4). A complete assignation of the ^{1}H-NMR spectral bands was performed and it is shown in the experimental section. The numbered scheme for NN ligands is shown in Fig. 1. The integration of the signals corresponding to the NN ligands with respect to the NBP ones confirmed the stoichiometry of the new compounds in solution. The chemical shift of the signals corresponding to the aliphatic protons of the NBP ligands (3.03 ppm (t, 2H), 2.00 (m, 4H) and 3.32 ppm (t, 2H), 2.26 (m, 2H) for ale and pam, respectively) was barely modified upon coordination as previously described for other NBP complexes [57, 60]. However, in all cases, the shape of the signals suffered from some modifications (broadening, changes in multiplicity) that could be attributed to the effect of palladium coordination.

^{31}P-{^{1}H}-NMR spectra of all the obtained complexes showed two signals at around 18 and 35 ppm (Fig.S5). This result is in accordance with two phosphorous populations for each compound that could be attributed to two not equivalent phosphorous atoms of each coordinated NBP but magnetically equivalent to the second coordinated NBP. A deshielding of the phosphorus nucleus should be expected due to the loss of the zwitterionic character of the NBP ligands due to coordination [66]. In addition, the different levels of protonation of the phosphonate groups as well as possible sodium interaction in solution could account for the observed results [57].

The stability of complexes in water was assessed by UV–Vis spectrophotometry and ^{1}H and ^{31}P NMR spectroscopy. The results obtained demonstrated that both compounds were stable in aqueous solutions during 24 h.

Biological results

Anti-*T. cruzi* activity

The activity against intracellular amastigote form of *T. cruzi* of the palladium complexes was studied. Results are shown in Table 1. All obtained complexes were inhibitors of *T. cruzi*'s growth and they resulted more active than the corresponding free NBP ligands. On the other hand, the antiparasitic activity seems to be dependent of the nature of the NN ligand. In fact, complexes with phen as ligand were 15 times more active than those including bpy. Pd–ale–phen and Pd–pam–phen were even more active than the reference drug benznidazole and almost 30 times more active than ale- and pam-free ligands. It also should be noted that these Pd–NBP–phen complexes only wed signs of unspecific toxicity on mammalian *Vero* cells at concentrations 40–70 times higher than the corresponding IC_{50} values (Table 1). An increase in the anti-*T. cruzi* activity and in selectivity as a consequence of complexation had already been reported by us for other metal–NBP compounds [12–14].

Anti-*T. gondii* activity

NBPs are also inhibitors of the growth of the protozoan parasite *Toxoplasma gondii*, causative agent of toxoplasmosis, a widespread disease that affects primarily immunocompromised and pregnant individuals [5]. In particular, ale and pam resulted effective in inhibiting intracellular proliferation of *T. gondii* showing IC_{50} values of 37 μM and 42 μM, respectively [67]. Based on that, obtained palladium complexes were tested against *T. gondii* tachyzoites. Pd–ale–phen and Pd–pam–phen complexes showed IC_{50} values of 15.2 ± 1.1 and 30.6 ± 1.2 μM, respectively. A slight increase in the activity was observed as a consequence of complexes' formation ($IC_{50} = 35$ μM for both free ale and free pam) [6]. Interestingly, no activity was observed for Pd–ale–bpy and Pd–pam–bpy complexes. A similar behavior was observed for the anti-*T. cruzi* activity, being complexes with phen as ligand more active than those with bpy.

Table 1 Results of biological and enzymatic assays

Compound	IC_{50} (μM)[a] *T. cruzi*	Toxicity (μM)[b] *Vero* cells	IC_{50} (μM)[c] *Tc*FPPS	IC_{50} (μM)[d] *h*FPPS	IC_{50} (μM)[e] *Tc*SPPS
ale	38.3 ± 2.3[f]	> 100	0.20 ± 0.05	1.52 ± 0.29	5.88 ± 1.53
Pd–ale–phen	1.44 ± 0.86	100	0.12 ± 0.01	0.40 ± 0.03	1.35 ± 0.12
Pd–ale–bpy	17.36 ± 0.48	100	0.33 ± 0.08	0.52 ± 0.04	0.96 ± 0.06
pam	38.8 ± 5.0[f]	> 100	0.05 ± 0.01	0.46 ± 0.07	0.99 ± 0.10
Pd–pam–phen	1.30 ± 0.77	50	0.22 ± 0.02	0.41 ± 0.09	0.57 ± 0.06
Pd–pam–bpy	21.4 ± 0.80	50	nd	nd	nd
Benznidazol	2.02 ± 0.32	–	–	–	–

Where indicated values are means ± s.d. of three independent experiments ($n = 3$)

nd not determined because of unspecific toxicity

[a]Concentration of compounds inhibiting 50% growth of *T. cruzi* amastigotes

[b]Concentration of compounds showing signs of toxicity on Vero cells (visual assay)

[c]Concentration of compounds inhibiting 50% activity of *Tc*FPPS

[d]Concentration of compounds inhibiting 50% activity of *Hs*FPPS

[e]Concentration of compounds inhibiting 50% activity of *Tc*SPPS

[f][12]

Correlation between anti-tumor and antiparasitic activities

Based on the proposed parallelism between the antitumor and antiparasitic effects [18–21], the cytotoxicity of the complexes on MG-63 osteosarcoma and the A549 lung adenocarcinoma cells was preliminary investigated. Results are shown in Fig. S6.

In A549 cells, Pd–ale–phen and Pd–pam–phen showed the highest cytotoxic activities. For this cell line, the tendency in cytotoxicity was similar to that observed for the antiparasitic activity. On the other hand, in MG-63 cells, only Pd–pam–phen showed cytotoxic effect while Pd–pam–bpy did not show any effects and Pd–ale–phen and Pd–ale–bpy only provoked a slight effect in the cell viability. As expected, on this bone-related cell line, the cytotoxic activity was dependent not only on the NN ligand but also on the NBP.

Although Pd–NBP–NN compounds were designed as potential antiparasitic agents, some of the obtained cytotoxic results were similar to those previously reported for some palladium and platinum complexes with NBPs as ligands [60, 68] and to the reference drug cisplatin (IC_{50} for A549 = 114.0 ± 9.1 μM [69] and IC_{50} for MG-63 = 39.0 ± 1.2 μM [70]). In addition, a quite good correlation between both activities was observed.

Insight into the potential targets

*Tc*FPPS, *Hs*FPPS and *Tc*SPPS inhibition assays

The main mode of anti-*T. cruzi* action of NBPs and their metal complexes has been related to the inhibition of farnesyl pyrophosphate synthase enzyme (*Tc*FPPS) [5, 12–14]. Therefore, the ability of the obtained palladium complexes to inhibit *Tc*FPPS was assayed. Results are depicted in Table 1. Studied complexes resulted in inhibitors of *Tc*FPPS but obtained IC_{50} values were comparable to those observed for the free NBP ligands. For other previously obtained metal compounds with NBPs as ligands, a fairly good correlation between the ability of the complexes to inhibit both intracellular *T. cruzi* amastigotes growth and *Tc*FPPS activity had been found [12, 13]. However, for the complexes described herein, *Tc*FPPS inhibition values could not explain the increase of the anti-*T. cruzi* activity as a consequence of complexes' formation.

On the other hand, solanesyl-diphosphate synthase (*Tc*SPPS) is an enzyme belonging to the prenyltransferase family involved in the biosynthesis of solanesyl diphosphate, a precursor of the side chains of ubiquinones. Because ubiquinones play a central role in energy production in parasites, *Tc*SPPS could be a promising chemotherapeutic target, in particular for bisphosphonates [54]. Both the free NBP ligands and palladium complexes showed inhibition of *Tc*SPPS (Table 1). The inhibition by Pd–ale–phen and Pd–ale–bpy were larger than the inhibition by ale ligand alone but did not correlate with the growth inhibition results. So, the inhibition of this enzyme could not either explain the differences between the anti-*T. cruzi* activity of the different palladium compounds.

Finally, complexes were also assayed on their ability to inhibit human farnesyl pyrophosphate synthase enzyme (*Hs*FPPS) (Table 1). Results showed that FPPS inhibition is not selective. In spite of that, most obtained palladium compounds were non-toxic for mammalian *Vero* cells at low concentrations.

DNA interaction

Fluorescence experiments

As stated, DNA could be a potential target for the title metal compounds not only through the palladium ion by covalent binding but also through the NN ligand in an intercalative-like mode. Therefore, the fluorescent DNA probe, ethidium bromide (EB), was used to access the interaction of the obtained complexes with DNA. EB is a conjugate planar molecule with weak intrinsic fluorescence emission. At pH 7.4 in Tris–HCl buffer, its spectrum shows an emission maximum at 601 nm (λexc. = 510 nm). Intercalation of EB into double-stranded DNA induces an increase of the fluorescence quantum yield [71]. In the spectrum of the {DNA–EB} adduct, the emission maximum is shifted to 594 nm under these experimental conditions. Neither DNA nor the palladium complexes are fluorescent and no fluorescence emission results from compounds' direct interaction with DNA.

Obtained results for the titration of the {DNA–EB} adduct with Pd–ale–phen and Pd–ale–bpy are shown as an example in Fig. S7. For Pd–ale–phen, a quenching of the emission of {DNA–EB} adduct up to 50% was observed upon increasing the complex's concentration. The decrease in emission intensity was accompanied by a small red shift of around 2 nm at the highest concentrations in accordance to the change from the characteristic emission of the {DNA–EB} adduct (594 nm) to the one of the free EB (601 nm) (Fig. S8). For Pd–ale–bpy, only a very slight effect on the emission intensity was observed (Fig. S7). A quite similar behavior is observed for Pd–pam–phen when compared to Pd–pam–bpy (Fig. S9). These results are consistent with an EB displacement from the {DNA–EB} adduct brought upon by the binding of Pd–NBP–phen complexes in an intercalative-like mode or by inducing DNA conformational changes, both mechanisms promoting the partial release of EB.

The extent of the interaction involved in the fluorescence quenching process for Pd–NBP–phen complexes can be assessed by a Stern–Volmer analysis according to the below equation:

$$IF_0/IF = 1 + K_{SV}[Q]. \quad (1)$$

In Eq. (1), IF_0 and IF are the emission fluorescence intensity of the {DNA–EB} adduct in the absence and in the presence of the complex, respectively, K_{SV} is the Stern–Volmer constant, and [Q] is the concentration of the quencher (in this case, the complexes) [56]. For both studied complexes, the plot IF_0/IF vs. [complex] showed a linear fit with logK_{SV} values of 4.6 and 3.5 for Pd–ale–phen and Pd–pam–phen, respectively. In the case of Pd–ale–phen the Stern–Volmer plot curves downward towards the x-axis at the highest concentrations which is a characteristic feature of two fluorophore populations, one of which is not accessible to the quencher [56].

Obtained results showed that, as expected, the nature of the NN ligand seems to determine the complexes' interaction with DNA. In fact, both Pd–NBP–phen complexes show a much higher affinity for DNA in the EB displacement reaction experiments than their Pd–NBP–bpy counterparts.

Conclusions

Four new palladium complexes with the bioactive bisphosphonates alendronate and pamidronate as ligands and phenanthroline and bipyridine as co-ligands were synthesized and fully characterized. All the obtained compounds showed an increased anti-*T. cruzi* activity when compared to the free NBP ligands. In particular, Pd–NBP–phen complexes resulted 15 times more active than the corresponding bpy analogs. This tendency was also observed for the anti-*T. gondii* and antitumor activities. However, all the complexes were able to similarly inhibit *Tc*FPPS and *Tc*SPPS enzymes suggesting that enzymatic inhibition could not be responsible for the observed differences in the biological activity of the obtained compounds. On the contrary, such differences could be related to their ability to interact with DNA in an intercalative-like manner. In the search of better compounds for the treatment of parasitic illnesses, the title palladium compounds are good candidates for further developments, in particular, for in vivo studies.

Acknowledgements We thank Melina Galizzi for technical help. Authors thank CSIC, PEDECIBA and ANII-SNI, Uruguay, and FONDECYT 1190340, Chile. Z-H Li and R.D. work was funded by the U.S. National Institute of Health (Grant AI082542 to R.D).

Compliance with ethical standards

Conflict of interest All authors declare that they have no conflict of interest.

References

1. Graham Russell R (2011) Bone 49:2–19
2. Gałęzowska J (2018) ChemMedChem 13(4):289–302
3. Ebetino FH, Hogan AML, Sun S, Tsoumpra MK, Duan X, Triffitt JT, Kwaasi AA, Dunford JE, Barnett BL, Oppermann U, Lundy MW, Boyde A, Kashemirov BA, McKenna ChE, Russell RG (2011) Bone 49:20–33
4. Cremers S, Drake MT, Ebetino FH, Bilezikian JP, Russell RGG (2019) Br J Clin Pharmacol 85(6):1052–1062
5. Docampo R, Moreno SN (2011) Curr Drug Target-Infect Disord 1:51–61

6. Martin MB, Grimley JS, Lewis JC, Heath HT, Bailey BN, Kendrick H, Yardley V, Caldera A, Lira R, Urbina JA, Moreno SNJ, Docampo R, Croft SL, Oldfield E (2001) J Med Chem 44(6):909–916
7. Urbina JA, Docampo R (2003) Trends Parasitol 19:495–501
8. Docampo R, Moreno SNJ (2008) Curr Pharm Des 14:882–888
9. Montalvetti A, Bailey BN, Martin MB, Severin GW, Oldfield E, Docampo R (2001) J Biol Chem 276:33930–33937
10. Rodriguez JB, Falcone BN, Szajnman SH (2016) Expert Opin Drug Discov 11:307–320
11. Mukherjee S, Basu S, Zhang K (2019) Mol Biochem Parasit 230:8–15
12. Demoro B, Caruso F, Rossi M, Benítez D, Gonzalez M, Cerecetto H, Parajón-Costa B, Castiglioni J, Gallizi M, Docampo R, Otero L, Gambino D (2010) J Inorg Biochem 104:1252–1258
13. Demoro B, Caruso F, Rossi M, Benítez D, González M, Cerecetto H, Galizzi M, Malayil L, Docampo R, Faccio R, Mombrú AW, Gambino D, Otero L (2012) Dalton Trans 41(21):6468–6476
14. Demoro B, Rostán S, Moncada M, Li ZH, Docampo R, Olea Azar C, Maya JD, Torres J, Gambino D, Otero L (2018) J Biol Inorg Chem 23(2):303–312
15. Cavalli A, Bolognesi ML (2009) J Med Chem 52:7339–7359
16. Zheng W, Zhao Y, Luo Q, Zhang Y, Wu K, Wang F (2016) Sci China Chem 59:1240–1249
17. Huang R, Wallqvist A, Covell DG (2005) Biochem Pharmacol 69:1009–1039
18. Kinnamon K, Steck EA, Rane ES (1979) Antimicrob Agents Chemother 15:157–160
19. Dorosti Z, Yousefi M, Maryam Sharafi S, Darani HY (2014) Future Oncol 10:2529–2539
20. Sánchez-Delgado RA, Anzellotti A, Suárez L (2004) Metal ions in biological systems. In: Sigel H, Sigel A (eds) 41: metal ions and their complexes in medication. Marcel Dekker, New York, pp 379–419
21. Otero L, Gambino D (2019) Metal compounds in the development of antiparasitic agents: rational design from basic chemistry to the clinic. In: Carver P (ed) 19: essential metals in medicine: therapeutic use and toxicity of metal ions in the clinic metal ions in life sciences. de Gruyter, Berlin, pp 331–358
22. Pages BJ, Garbutcheon-Singh KB, Aldrich-Wright JR (2017) Eur J Inorg Chem 2017(12):1613–1624
23. Fanelli M, Formica M, Fusi V, Giorgi L, Micheloni M, Paoli P (2016) Coord Chem Rev 310:41–79
24. Scalese G, Benítez J, Rostán S, Correia I, Bradford L, Vieites M, Minini L, Merlino A, Coitiño EL, Birriel E, Varela J, Cerecetto H, González M, Costa Pessoa J, Gambino D (2015) J Inorg Biochem 147:116–125
25. Gambino D (2011) Coord Chem Rev 255(19–20):2193–2203
26. Scalese G, Mosquillo MF, Rostán S, Castiglioni J, Alho I, Pérez L, Correia I, Marques F, Costa Pessoa J, Gambino D (2017) J Inorg Biochem 175:154–166
27. Alam MN, Huq F (2016) Coord Chem Rev 316:36–67
28. Otero L, Vieites M, Boiani L, Denicola A, Rigol Olsen C, Opazo L, Olea Azar C, Maya Arango J, Morello Casté A, Krauth Siegel R, Piro O, Castellano E, González M, Gambino D, Cerecetto H (2006) J Med Chem 49(11):3322–3331
29. Rodríguez Arce E, Mosquillo MF, Pérez-Díaz L, Echeverría GA, Piro OE, Merlino A, Coitiño EL, Maríngolo Ribeiro C, Leite CQF, Pavan FR, Otero L, Gambino D (2015) Dalton Trans 44:14453–14464
30. Rodríguez Arce E, Putzu E, Lapier M, Maya JD, Olea Azar C, Echeverría GA, Piro OE, Medeiros A, Sardi F, Comini M, Risi G, Correia I, Costa Pessoa J, Otero L, Gambino D (2019) Dalton Trans 48:7644–7658
31. Garoufis A, Hadjikakou SK, Hadjiliadis N (2009) Coord Chem Rev 253(9–10):1384–1397
32. Mansouri-Torshizi H, Saeidifar M, Divsalar A, Saboury AA (2010) Spectrochim Acta A 77(1):312–318
33. Kukushkin YN, Vlasova RA, Pazukhina YL (1968) Zh Prikl Khim 41(11):2381–2385
34. Fulmer GR, Miller AJ, Sherden NH, Gottlieb HE, Nudelman A, Stoltz BM, Bercaw JE, Goldberg KI (2010) Organometallics 29(9):2176–2179
35. Becke AD (1993) J Chem Phys 98:1372–1377
36. Becke AD (1988) Phys Rev A 38:3098–3100
37. Lee C, Yang W, Parr RG (1988) Phys Rev B 37:785–789
38. Hariharan PC, Pople JA (1973) Theoret Chim Acta 28:213–222
39. Francl MM, Petro WJ, Hehre WJ, Binkley JS, Gordon MS, DeFrees DJ, Pople JA (1982) J Chem Phys 77:3654–3665
40. Feller D (1996) J Comp Chem 17:1571–1586
41. Schuchardt KL, Didier BT, Elsethagen T, Sun L, Gurumoorthi V, Chase J, Li J, Windus TL (2007) J Chem Inf Model 47:1045–1052
42. Matczak-Jon E, Videnova-Adrabinska V (2005) Coord Chem Rev 249:2458–2488
43. Hay PJ, Wadt WR (1985) J Chem Phys 82:270–283
44. Hay PJ, Wadt WR (1985) J Chem Phys 82:284–298
45. Hay PJ, Wadt WR (1985) J Chem Phys 82:299–310
46. Pyykkö P (1990) The effect of relativity in atoms, molecules and the solid state. Plenum, New York
47. Frisch MJ, Trucks GW, Schlegel HB, Scuseria GE, Robb MA, Cheeseman JR, Scalmani G, Barone V, Petersson GA, Nakatsuji H, Li X, Caricato M, Marenich A, Bloino J, Janesko BG, Gomperts R, Mennucci B, Hratchian HP, Ortiz JV, Izmaylov AF, Sonnenberg JL, Williams-Young D, Ding F, Lipparini F, Egidi F, Goings J, Peng B, Petrone A, Henderson T, Ranasinghe D, Zakrzewski VG, Gao J, Rega N, Zheng G, Liang W, Hada M, Ehara M, Toyota K, Fukuda R, Hasegawa J, Ishida M, Nakajima T, Honda Y, Kitao O, Nakai H, Vreven T, Throssell K, Montgomery JA, Peralta JE Jr, Ogliaro F, Bearpark M, Heyd JJ, Brothers E, Kudin KN, Staroverov VN, Keith T, Kobayashi R, Normand J, Raghavachari K, Rendell A, Burant JC, Iyengar SS, Tomasi J, Cossi M, Millam JM, Klene M, Adamo C, Cammi R, Ochterski JW, Martin RL, Morokuma K, Farkas O, Foresman JB, Fox DJ (2013) Gaussian 09, Rev. A.01. Gaussian Inc, Wallingford
48. Canavaci AM, Bustamante JM, Padilla AM, Pereza Brandan CM, Simpson LJ, Xu D, Boehlke CL, Tarleton RL (2010) PLOS Negl Trop Dis 4:e740–e745
49. Recher M, Barboza AP, Li Z-H, Galizzi M, Ferrer-Casal M, Szajnman SH, Docampo R, Moreno SNJ, Rodriguez JB (2013) Eur J Med Chem 60:431–440
50. Mosmann TJ (1983) Immunol Methods 65(1–2):55–63
51. Nardelli SC, Che FY, Silmon de Monerri NC, Xiao H, Nieves E, Madrid-Aliste C, Angel SO, Sullivan WJ Jr, Angeletti RH, Kim K, Weiss LM (2013) MBio 4(6):e00922–1013
52. Kavanagh KL, Guo K, Dunford JE, Wu X, Knapp S, Ebetino FH, Rogers MJ, Russell RG, Oppermann U (2006) Proc Natl Acad Sci USA 103:7829–7834
53. Rilling HC (1985) Methods Enzymol 110:145–152
54. Ferella M, Montalvetti A, Rohloff P, Miranda K, Fang J, Reina S, Kawamukai M, Búa J, Nilsson D, Pravia C, Katzin A, Cassera MB, Åslund L, Andersson B, Docampo R, Bontempi EJ (2006) J Biol Chem 281(51):39339–39348
55. Barton JK, Goldberg JM, Kumar ChV, Turro NJ (1986) J Am Chem Soc 108:2081–2088
56. Lakowicz JR (2006) Principles of fluorescence spectroscopy, 3rd edn. Springer, New York **(ch. 8)**
57. Margiotta N, Capitelli F, Ostuni R, Natile G (2008) J Inorg Biochem 102(12):2078–2086
58. Wimmer S, Castan P, Wimmer FL, Johnson NP (1989) J Chem Soc Dalton Trans 403–412
59. Galezowska J, Gumienna-Kontecka E (2012) Coord Chem Rev 256:105–124

60. Fathy AA, Butler IS, Abd Elrahman M, Jean-Claude BJ, Mostafa SI (2018) Inorg Chim Acta 473:44–50
61. Campos-Vallette MM, Clavijo RE, Mendizabal F, Baraona R, Zamudio W, Diaz G (1996) Vib Spectrosc 12(1):37–44
62. Gong Y, Tang W, Hou W, Zha Z, Hu C (2006) Inorg Chem 45:4987–4995
63. Juribašić M, Tušek-Božić L (2009) J Mol Struct 924–926:66–72
64. Barone V, Cossi M (1998) J Phys Chem A 102:1995–2001
65. Cossi M, Rega N, Scalmani G, Barone V (2003) J Comp Chem 24:669–681
66. Appleton G, Hall JR, McMahon I (1986) Inorg Chem 25:726–734
67. Rodrigues CD, Scott DA, Bailey BN, De Souza W, Benchimol M, Moreno B, Urbina JA, Oldfield E, Moreno SNJ (2000) Biochem J 349(3):737–745
68. Alvarez-Valdes A, Matesanz AI, Perles J, Fernandes C, Correia JDG, Mendes F, Quiroga AG (2019) J Inorg Biochem 191:112–119
69. Frik M, Martínez A, Elie BT, Gonzalo O, Ramírez de Mingo D, Sanaú M, Sánchez Delgado R, Sadhukha T, Prabha S, Ramos JB, Marzo I, Contel M (2014) J Med Chem 57(23):9995–10012
70. Burgos Lopez Y, Del Plá J, Balsa LM, León IE, Echeverría GA, Piro OE, García Tojal J, Pis Diez R, González Baró AC, Parajón-Costa BS (2019) Inorg Chim Acta 487:31–40
71. Tan C, Liu J, Chen LM, Shi S, Ji LN (2008) J Inorg Biochem 102:1644–1653

Affiliations

Micaella Cipriani[1] · Santiago Rostán[1] · Ignacio León[2] · Zhu-Hong Li[3] · Jorge S. Gancheff[1] · Ulrike Kemmerling[4] · Claudio Olea Azar[5] · Susana Etcheverry[2] · Roberto Docampo[3] · Dinorah Gambino[1] · Lucía Otero[1]

[1] Química Inorgánica, Facultad de Química, UdelaR, Montevideo, Uruguay

[2] Facultad de Ciencias Exactas, Centro de Química Inorgánica (CONICET-UNLP), Universidad Nacional de La Plata, La Plata, Argentina

[3] Center for Tropical and Emerging Global Diseases and Department of Cellular Biology, University of Georgia, Athens, USA

[4] Programa de Anatomía Y Biología del Desarrollo, Facultad de Medicina, ICBM, Universidad de Chile, Santiago, Chile

[5] Departamento de Química Inorgánica Y Analítica, Facultad de Ciencias Químicas Y Farmacéuticas, Universidad de Chile, Santiago, Chile